

Optimization of the Ballistic Guide Design for the SNS FNPB 8.9 Å Neutron Line

Takeyasu M. Ito ^{*,1} Christopher B. Crawford,
Geoffrey L. Greene

*The Department of Physics and Astronomy, The University of Tennessee
Knoxville, TN 37996
and
Physics Division, Oak Ridge National Laboratory, Oak Ridge, TN, 37831*

Abstract

The optimization of the ballistic guide design for the SNS Fundamental Neutron Physics Beamline 8.9 Å line is described. With a careful tuning of the shape of the curve for the tapered section and the width of the straight section, this optimization resulted in more than 75% increase in the neutron flux exiting the 33 m long guide over a straight $m = 3.5$ guide with the same length.

Key words: Neutron beam line, ballistic guide, Monte Carlo simulation

1 Introduction

Recent years have seen a remarkable progress in the technology of producing supermirrors, both in terms of the critical angle and the reflectivity, which resulted in substantial increase in neutron flux at various neutron beam facilities. However, for transporting neutrons over long distances ($\gtrsim 30$ m), the finite reflectivity for angles above θ_c (the critical angle for natural nickel) causes a significant loss in the neutron flux exiting the guide. (The reflectivity of a good $m = 3.5$ guide is 80% at $m = 3.5$).

The so-called “ballistic guide” geometry, first proposed by Mezei [1], allows neutrons to be transported over long distances without significant losses. We

* Corresponding author

Email address: ito@lanl.gov (Takeyasu M. Ito).

¹ Present address: Los Alamos National Laboratory, Los Alamos, NM 87545

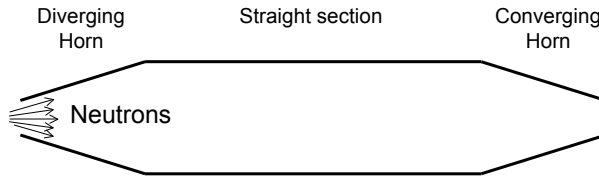


Fig. 1. Schematic of a ballistic guide

have performed a careful optimization of the ballistic guide design for the SNS FNPB 8.9 Å Neutron Beam Line using a custom made Monte Carlo simulation program. With a careful tuning of the shape of the curve for the tapered section and the width of the straight section, this optimization resulted in more than a 75% increase in the neutron flux exiting the 33 m long guide over that of a straight $m = 3.5$ guide with the same length. In this paper, we describe the optimization process and present the obtained results. One important point that needs to be emphasized is that the optimum choice for various aspects of the ballistic guide geometry, such as the shape of the tapered section and the widths of the straight section, strongly depends on the angular and positional distribution of the neutron flux entering the ballistic guide.

This paper is structured as follows. In section 2, the principle of the ballistic guide and some important design considerations are reviewed. Then in section 3, after a brief description of the SNS FNPB beamline and its characteristics, the optimization process including the Monte Carlo program is described in detail, and the results are presented.

2 General Consideration

2.1 Ballistic guide – the principle and some design considerations

The term “ballistic guide” refers to an arrangement in which a diverging horn is followed by a wide (and usually long) straight section, and then by a converging horn (see Fig. 1). With such an arrangement, the divergence (angular spread) of the incident neutron distribution is turned to a spatial spread by the diverging horn, which results in a reduced loss during the propagation through the straight section because of the smaller angles (i.e. higher reflectivity) and fewer bounces (due to the smaller angles and the larger guide width).

Liouville’s theorem states that the following inequality holds for the phase space occupied by an ensemble of neutrons traveling through a ballistic guide:

$$\Delta\theta_i \cdot \Delta x_i \leq \Delta\theta_S \cdot \Delta x_S, \quad (1)$$

and where $\Delta\theta_i$ and Δx_i are the angular and spatial spreads of the initial distribution of the neutrons entering the diverging horn of the ballistic guide, and $\Delta\theta_S$ and Δx_S are those for the neutrons in the straight section right after the diverging horn. A similar inequality holds for the neutrons in the straight section right before the converging horn and the neutrons exiting the converging horn. Note, however, in general in both the diverging and converging horns, there is an unavoidable loss of neutron flux due to the fact that the reflectivity is less than unity for angles larger than θ_c . In fact, as we will see later, the loss in the diverging horn is a major source of loss in ballistic guide geometry.

The task of optimizing the design is to perform this “phase space rotation” (from large $\Delta\theta_i$ and small Δx_i to small $\Delta\theta_S$ and large Δx_S) in the diverging horn as efficiently as possible, i.e. as closely to the equality limit as possible, while minimizing the loss (due to the finite reflectivity) in the diverging horn itself. An inefficient phase space rotation would result in a larger than necessary guide width for the straight section, which would not only be more expensive to build but would also cause a larger loss in the converging horn. Also, the shape of the converging horn has to be optimized to minimize additional losses during the second phase space rotation.

The converging horn does not exactly reverse the effect of the diverging horn on the neutron phase space. Rather, a loss of neutrons also occurs in the converging horn, due to the nonlinear nature of ballistic transport. The loss in the converging horn is another major contributor to the loss in the ballistic guide. This point is illustrated in Fig. 2, where the red and blue lines represent the trajectories of two neutrons that had slightly different initial conditions (the neutrons travel from left to right). Despite the small difference in the initial conditions, one (red) makes it to the end whereas the other (blue) does not (these trajectories were calculated by the simulation program described in this document). The neutron represented by the blue trajectory gets lost when it makes the second interaction with the wall of the converging horn, where the angle was too large for the neutron to be reflected (the first interaction in the converging horn has the same angle as that in the diverging horn). It can also be seen that the neutron with the blue trajectory too would make it to the end without making the second interaction with the wall in the converging horn, if the straight section were a little shorter or the neutron started at a slightly different location.

For a typical supermirror, the reflectivity is virtually unity for angles less than θ_c . Therefore, $\Delta\theta_S$ does not have to be infinitesimally small. It should rather be around θ_c . Otherwise Δx_S would be unnecessarily large, which would cause a larger loss in the converging horn. This argument provides a good estimate for the optimum guide width of the straight section. In general, if the input neutron distribution has an angular spread that extends to $m_i \times \theta_c$, then,

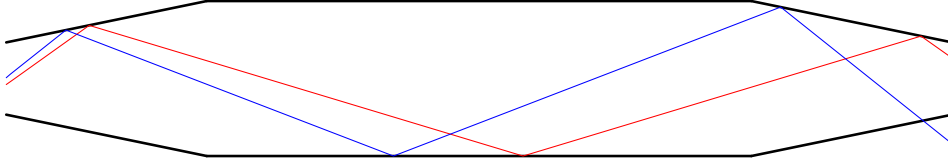


Fig. 2. Illustration of how the converging horn does not do the exact reverse of the diverging horn because of the non point-source nature of the distribution (see main text).

the optimum guide width is expected to be in the neighborhood of m_i times the width of the entrance of the diverging horn (or perhaps slightly narrower, because the narrower the guide is in the straight section, the smaller the loss is in the converging horn).

2.2 Curved taper

The simplest realization of a ballistic guide uses a straight taper for the diverging and converging horns. However, a more efficient phase space rotation of Eq. (1) can be achieved by using a curved taper as depicted in Fig. 3. This figure 3 illustrates how the use of a curved taper for the diverging horn can result in a smaller loss in the horn and in a more favorable neutron angular distribution in the straight section. The blue arrow represents a trajectory of a neutron with a large angle. It would hit the wall of the horn at a larger angle at point a' for the straight taper than it would at point a for the curved taper. Since the reflectivity is larger for smaller angles of incident (when the angle is larger than θ_c), the curved taper causes a smaller loss for large angle neutrons than the straight taper. The red arrow represents a trajectory of a neutron with a small angle. In this case, the neutron would hit the wall at a larger angle for the curved taper than it would for the straight taper. However, in this case, the angle is already small (smaller than θ_c) so hitting the wall at a larger angle does not lead to a loss. Instead, the final angle resulting from the bounce is closer to being parallel to the z axis for the curved taper, which results in a reduced loss in the converging horn. (Note if all the neutrons have a trajectory parallel to the z axis, the loss in the converging horn is substantially reduced.)

We therefore considered using a curved taper for the diverging and converging horns in this study. As is obvious from the discussion in the previous paragraph, the shape of the curved taper has to be optimized for the given neutron distribution. To conveniently parameterize the shape of the curve, we used the following expression for the shape of curved tapers:

$$x = \frac{(X2 - X1)}{L}z + X1 - a\frac{z - L}{L}\frac{z}{L}|X2 - X1|, \quad (2)$$

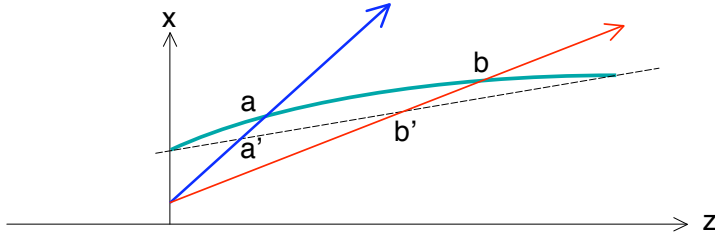


Fig. 3. Comparison between a curved and a straight taper. The curved taper is represented by the light green curve. The back straight line represents the straight taper. The blue and red arrows represent neutrons coming in at large and small angles, respectively.

where $X1$ and $X2$ are the half width of the entrance and exit of the horn and L is the length of the horn, as shown in Fig. 4. The neutron beam travels in the positive z direction in this figure, and x is perpendicular to z . Note that the first two terms of Eq. (2) give the straight line that connects the two points determined by the entrance and exit widths and the length of the horn. The third term is a quadratic in z , fixed at the endpoints, which represents the first order deviation from the straight line. The dimensionless parameter a determines the size of this term: $a = 0$ corresponds to the straight line, and $a = 1$ corresponds to matching the derivative at the end of the horn with the straight section. It gives a curve that deviates from the straight line by $\frac{|X2-X1|}{4}$ at $z = L/2$ (note that both the factor z and $z - L$ are divided by L so that a is dimensionless).

There is no point in using a parabola, since the source is not point-like. The advantage of using this parameterization, instead of using parabola, hyperbola, or ellipsoid, is that it is linear in the limit of $a = 0$ instead of in the asymptotic limit of some parameter $p \rightarrow \infty$. No matter which shape we use – parabola, hyperbola, or ellipsoid – the actual deviation from the straight line will be small because the horn is several meters long whereas it is only a few tens of centimeters wide. Therefore our parameterization should capture the essence of the curved guide. In other words, we do not expect the results to be too dependent of the details of the shape, which was confirmed for our particular neutron distribution by adding terms in higher order in z and seeing no significant gain in performance (see Section 3.5).

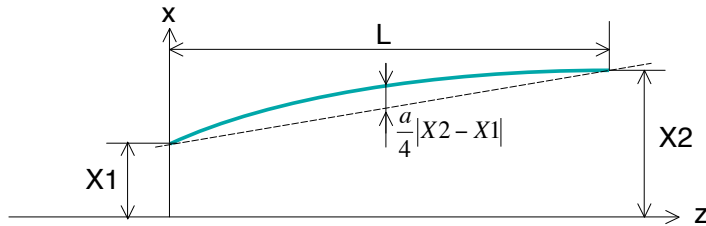


Fig. 4. Parameterization used for curved tapers in this study (see the main text).

3 Optimization of the FNPB 8.9 Å beamline

3.1 SNS and FNPB

The Spallation Neutron Source (SNS), currently under construction at the Oak Ridge National Laboratory, is an accelerator-based neutron source, and will provide the world’s most intense pulsed neutron beams for scientific research and industrial development [2]. The Fundamental Neutron Physics Beamline (FNPB), one of the 24 neutron beamlines in the SNS target hall, is dedicated to fundamental physics using cold and ultracold neutrons. Figure 5 shows the schematic of the layout of the FNPB beamline. The FNPB has two neutron beamlines, the “Cold Neutron Line” and the 8.9Å Line (or “UCN Line”). The 8.9Å Line is dedicated to experiments that will use the superthermal process in superfluid liquid helium to produce ultra-cold neutrons. The 8.9Å neutrons will be selected by a double crystal monochromator and will be sent to an external building located about 30 m downstream.

A calculation [4] shows that a neutron fluence of 0.94×10^9 n/s/Å can be obtained when a straight $m = 3.5$ guide with a cross section of 12 cm \times 14 cm and a length of 33 m is used to transport the 8.9Å neutrons from the monochromator to the external building. The goal of this study is to find the optimum geometry for a ballistic guide which transports the 8.9Å neutrons from the monochromator to the external building.

3.2 Characteristics of the incident neutron distribution

As mentioned in Section 2, the optimum choice for various aspects of the ballistic guide geometry, such as the shape of the tapered section and the widths of the straight section, strongly depends on the angular and position distribution of the neutron flux entering the ballistic guide. It is therefore important to examine the characteristics of the incident neutron distribution in order to

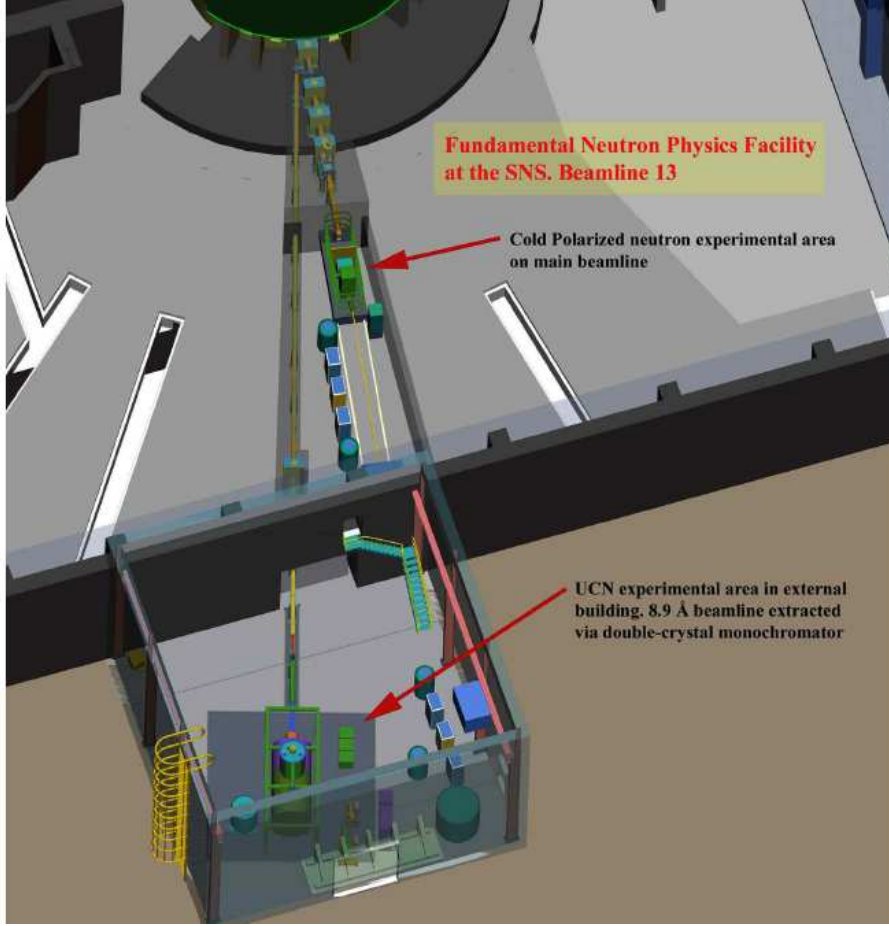


Fig. 5. Schematic of the layout of the Fundamental Neutron Physics Facility at the SNS.

intelligently optimize the design of the ballistic guide. Figures 6 and 7 show the position and angular distribution in the horizontal (x) and vertical (y) directions of the neutrons coming out of the double crystal monochromator. These distributions were obtained from a Monte Carlo program written by P. Huffman based on MCSTAS [5], which generates neutrons according to the neutron input source files for the SNS target and tracks neutrons through the FNPB beamline elements including the double crystal monochromator that extracts the 8.9 Å neutrons [4].

The position distributions shown in Fig. 6 confirm that the choice of the cross section of 12 cm \times 14 cm for the entrance of the ballistic guide is reasonable.

For the angular distributions, from Fig. 7 we notice that the horizontal angular spread is only $|\Delta\theta_x| < 2\theta_c$ whereas the vertical angular spread is as large as $|\Delta\theta_y| \sim 4\theta_c$. This is because of the mosaic structure of the crystals that are used in the double crystal monochromator, and also because of how the two crystals are arranged in the double crystal monochromator. The angular

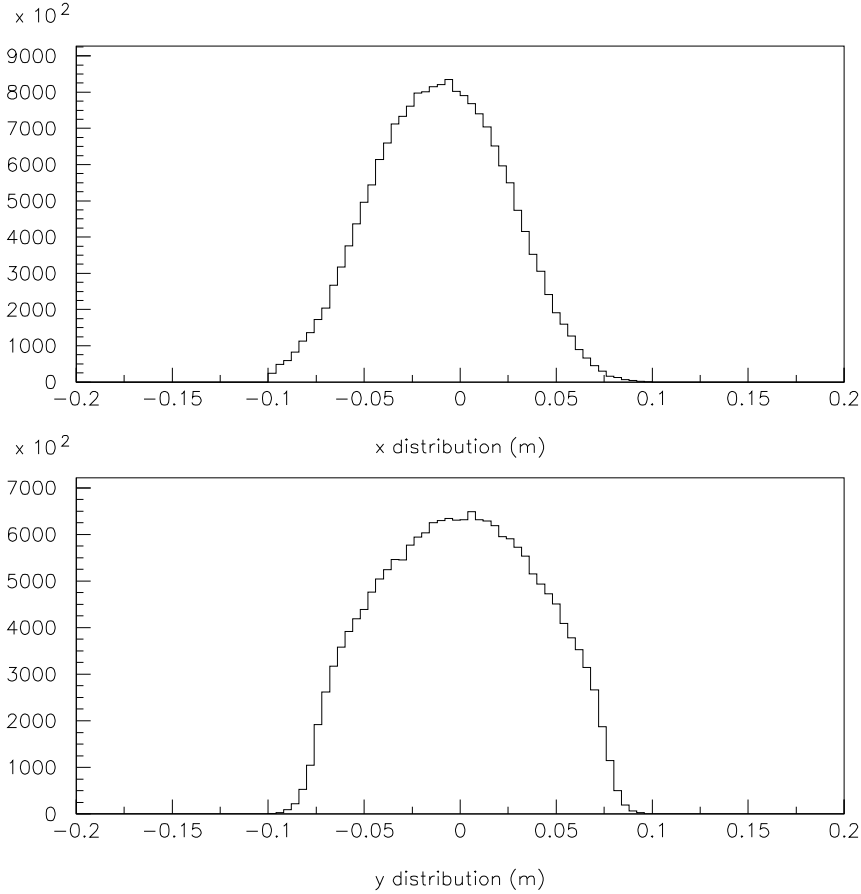


Fig. 6. Horizontal (top) and vertical (bottom) position distributions of the neutrons coming out of the double crystal monochromator

spread caused by the randomly oriented small “blocks” in the mosaic of one crystal cancels that of the other crystal to the first order in the horizontal direction but not in the vertical direction when the two crystals are arranged horizontally. The narrow horizontal angular distribution also indicates that the neutron guide upstream of the double crystal monochromator is long enough for the neutrons with large angles be lost while they travel from the SNS target to the monochromator.

The implication of these two angular distributions to the design of the ballistic guide is as follows (see Fig. 8 for the notation):

- For the horizontal direction, from Eq. (1) and the succeeding argument, the optimum width of the straight section is expected to be $XW2 \sim 2 \times XW1 = 24$ cm.
- Also, since the angular spread is relatively small in the horizontal direction, it is expected that the supermirror coating can have a smaller value for m on the side walls of the diverging horn.

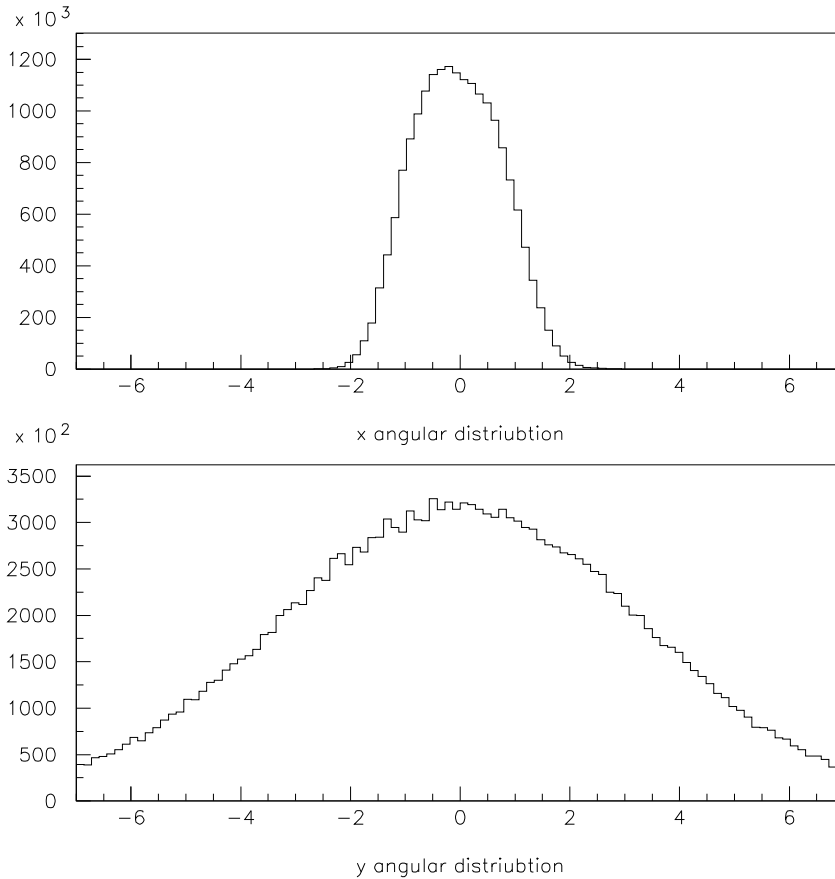


Fig. 7. Horizontal (top) and vertical (bottom) angular distributions of the neutrons coming out of the double crystal monochromator. The angles are in the unit of θ_c .

- On the other hand, in the vertical direction, because of the large angular spread, the width of the straight section should ideally be $YW2 \sim 4 \times YW1 = 56$ cm. However, it is mechanically limited to ~ 30 cm.

As discussed in Section 3.3, we varied $XW2$ between 15 cm and 30 cm in search of the optimum ballistic guide design.

We note that the angular spread could be reduced by using graphite crystals with a smaller mosaic angle [6].

3.3 Simulation program

The optimization of the ballistic guide was performed using a Monte Carlo simulation. A new neutron ray tracing package, dubbed NEUTRACK 8.9, was written to perform a series of transmission calculations to optimize the ballis-

tic guide for the 8.9 Å line. While there was already an MCSTAS program to simulate the whole FNPB beamline system, we decided that it was advantageous to develop a new ray tracing package and write a whole new program using it to design the 8.9 Å line for several reasons, including the following:

- The MCSTAS FNPB simulation tracks neutrons all the way from the SNS target down to the end of the beam line for all wavelengths. The fraction of the neutrons that get selected by the monochromator and get sent to the 8.9 Å line is very small. However, optimizing the ballistic guide design only involve simulating neutrons downstream of the monochromator. The simulation can be done more efficiently if the program simulates only the components downstream of the monochromator, generating only 8.9 Å neutrons at the entrance to the ballistic guide.
- Information important in designing a ballistic guide – such as, where exactly in the system neutrons are lost and what the distribution is like for the angle at which the neutrons interact with each segment of supermirror – is not easily accessible by the user in MCSTAS.

NEUTRACK 8.9 is designed to simulate only a single wavelength of neutrons. The user has a complete access to information such as where exactly in the system neutrons are lost and what the distribution is like for the angle at which the neutrons interact with each segment of supermirror.

A Monte Carlo simulation program using NEUTRACK 8.9 was written to simulate a ballistic guide for the 8.9 Å line. Neutrons were generated so that their distribution reproduces that of the neutrons coming out of the double crystal monochromator calculated by the MCSTAS FNPB simulation. The neutrons were then introduced into the ballistic guide, and the behavior of the neutrons in the guide was simulated. The performance of various geometries was evaluated using the transmission (TXMIT) – the ratio of the number of neutrons exiting the guide to the number of neutrons entering the guide – and the relative transmission (rel. TXMIT) – the ratio of the transmission of the guide geometry under consideration to that of the 12 cm × 14 cm straight guide. (Note that since the input to the ballistic guide is the same for all different geometries, the relative transmission is the same as the output neutron flux or fluence normalized to that of the straight guide.)

Various parameters including properties of the supermirrors were adjusted so that the results of this 8.9 Å line simulation program agreed with those from the MCSTAS FNPB simulation program for the same ballistic guide geometry. It was confirmed for several selected geometries that the results for the relative transmission from both simulation programs for the same geometry agreed within the statistical error of the simulation ($\sim 1\%$) as shown in Table 1. It was important to reproduce the input neutron distributions obtained from the MCSTAS FNPB simulation in the 8.9 Å line simulation, including the

Table 1

Comparison between MCSTAS and NEUTRACK 8.9. [Description of the guide geometries (for the parameter definition, see Table 2): a) straight guide with a 12 cm \times 14 cm cross section, $m = 3.5$ for all four walls; b) ballistic guide with straight taper with $L1 = L3 = 9$ m, $XW2 = 30$ cm, $m1_{TB} = m1_{LR} = 3.5$, $m2_{TB} = m2_{LR} = 2.0$, $m3_{TB} = m3_{LR} = 3.5$; c) ballistic guide with curved taper with $L1 = L3 = 9$ m, $XW2 = 30$ cm, $m1_{TB} = m1_{LR} = 3.5$, $m2_{TB} = m2_{LR} = 2.0$, $m3_{TB} = m3_{LR} = 3.5$, $a_H = a_V = 1.0$; d) ballistic guide with curved taper with $L1 = L3 = 7$ m, $XW2 = 20$ cm, $m1_{TB} = m1_{LR} = 3.5$, $m2_{TB} = m2_{LR} = 2.0$, $m3_{TB} = m3_{LR} = 3.5$, $a_H = 0.3$, $a_V = 1.1$.]

Guide	MCSTAS		NEUTRACK 8.9	
	TXMIT	rel. TXMIT	TXMIT	rel. TXMIT
a) Straight guide	0.3854(24)	1.000	0.3976(5)	1.000
b) Ballistic, straight taper	0.5827(31)	1.512(12)	0.6031(5)	1.517(2)
c) Ballistic, curved taper	0.6375(32)	1.654(13)	0.6611(5)	1.663(2)
d) Ballistic, curved taper, narrow	0.6759(33)	1.754(14)	0.6976(5)	1.755(2)

correlation between the vertical position and the vertical angle to obtain an agreement between the two simulation programs. Because of the simplicity of NEUTRACK 8.9 and because the 8.9 Å line simulation program only simulates the 8.9 Å line downstream of the monochromator, it is a more than two orders of magnitude faster than the MCSTAS FNPB simulation program to obtain results with the same statistical precision.

3.4 Physics-motivated optimization

Monte Carlo simulations were performed for various ballistic guide geometries to find the optimum geometry [high performance (= high transmission) and low cost]. We first performed an optimization in which the ranges of various parameters were selected based on the considerations given in Section 2.

The parameters used to describe the ballistic guide geometry are listed in Table 2 along with the value for the fixed parameters or the range of variation for optimized parameters. Some of the parameters are illustrated in Fig. 8. The values and the ranges for the parameters reflect various boundary conditions (e.g. the largest guide width practically possible is ~ 30 cm) and considerations (such as those discussed in Sections 2.1 and 3.2). For this study the length of the converging horn $L3$ was set to be the same as the length of the diverging horn $L1$ since no significant gain was seen when $L3$ was varied independent of $L1$ in a preliminary study.

Table 2

Parameters used to describe the ballistic guide geometry. The taper curvature parameters a_H and a_V are common for the diverging and converging horns.

Parameter	Description	Value
$L1$	length of the diverging horn	5, 6, 7, 8, 9 m
$L2$	length of the straight section	33 m $-(L1 + L3)$
$L3$	length of the converging horn	$L3 = L1$
$XW1$	width of the entrance	12 cm (fixed)
$XW2$	width of the straight section	15 cm – 30 cm
$XW3$	width of the exit	12 cm (fixed)
$YW1$	height of the entrance	14 cm (fixed)
$YW2$	height of the straight section	30 cm (fixed)
$YW3$	height of the exit	14 cm (fixed)
a_H	curvature parameter for the horns (left and right walls)	0 – 1.5
a_V	curvature parameter for the horns (top and bottom walls)	0 – 1.5
$m1_{TB}$	m for the diverging horn, top and bottom walls	3.5
$m1_{LR}$	m for the diverging horn, left and right walls	2.0, 3.5
$m2_{TB}$	m for the straight section, top and bottom walls	2.0
$m2_{LR}$	m for the straight section, left and right walls	1.5, 2.0
$m3_{TB}$	m for the converging horn, top and bottom walls	3.5
$m3_{LR}$	m for the converging horn, left and right walls	2.0, 3.5

When performing Monte Carlo simulation for geometries with curved taper, the curved taper was approximated by a series of short segments with straight tapers at different angles. Usually, each horn was divided into five segments to keep the computation time short (the computation time scales approximately as the number of the mirror segments). For a few selected geometries, a finer division was also tried. Results from five segments agreed with results from fourteen segments (for $L1 = 7$ m this corresponds to 50 cm long segments) within 1%.

The dependence of the relative transmission on $L1$ ($=L3$) and $XW2$ is shown in Fig. 9 for geometries with straight taper and in Fig. 10 for geometries with curved taper. For curved taper, the curvature parameters a_H and a_V were optimized for each combination of $L1$ and $XW2$. We found that the optimum values of a_H and a_V do not have a strong dependence on $XW2$, but do depend

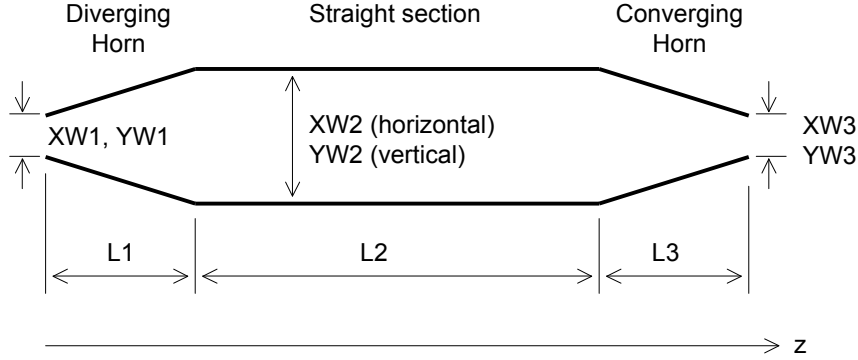


Fig. 8. Schematic of a ballistic guide with parameters used to describe the geometry

Table 3

Optimum values for a_H and a_V for different values of $L1$

$L1$	a_H	a_V
5 m	0.4	0.7
6 m	0.4	0.9
7 m	0.3	1.1
8 m	0.6	1.3
9 m	0.4	1.4

on the value of $L1$. The optimum values of a_H and a_V for different values of $L1$ are listed in Table 3.

For all the results plotted in these two Figures, the following values of m were used for the supermirror coating: $m1_{TB} = 3.5$, $m1_{LR} = 2.0$, $m2_{TB} = 2.0$, $m2_{LR} = 1.5$, $m3_{TB} = 3.5$, $m3_{LR} = 3.5$. We now discuss how each of these parameters was optimized. Because of the large vertical angular spread of the initial neutron distribution, it is important to use as high an m as possible for the top and bottom walls of the diverging horn ($m1_{TB} = 3.5$). However, because of the rather narrow horizontal divergence of the initial neutron distribution, it is not necessary to use as high an m for the side walls. In fact, reducing $m1_{LR}$ down to 2.0 from 3.5 did not lead to any reduction of the output neutron flux. This can also be seen from Fig. 11, which shows a distribution of the incident angle of the neutrons on the side wall of the diverging horn. It is seen that there are hardly any neutrons incident on the side wall of the diverging horn with an angle larger than $2 \times \theta_c$. For the straight section, the values for the m were determined to be $m2_{TB} = 2.0$ and $m2_{LR} = 1.5$ by looking at the the horizontal and vertical angular distributions

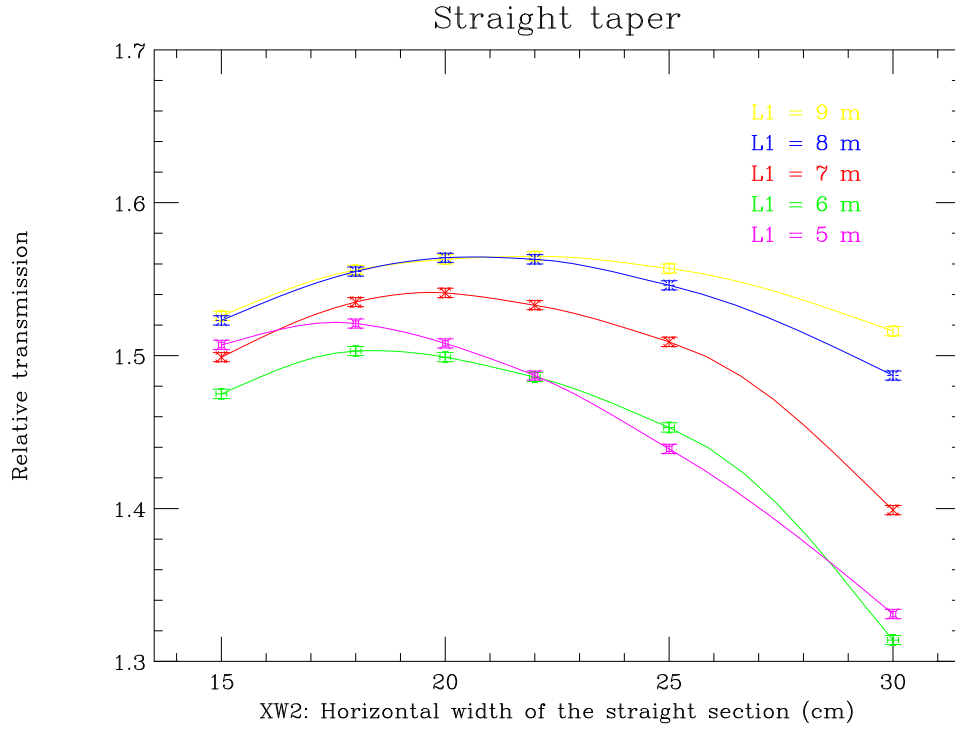


Fig. 9. Relative transmission vs horizontal width of the straight section for geometries with straight taper.

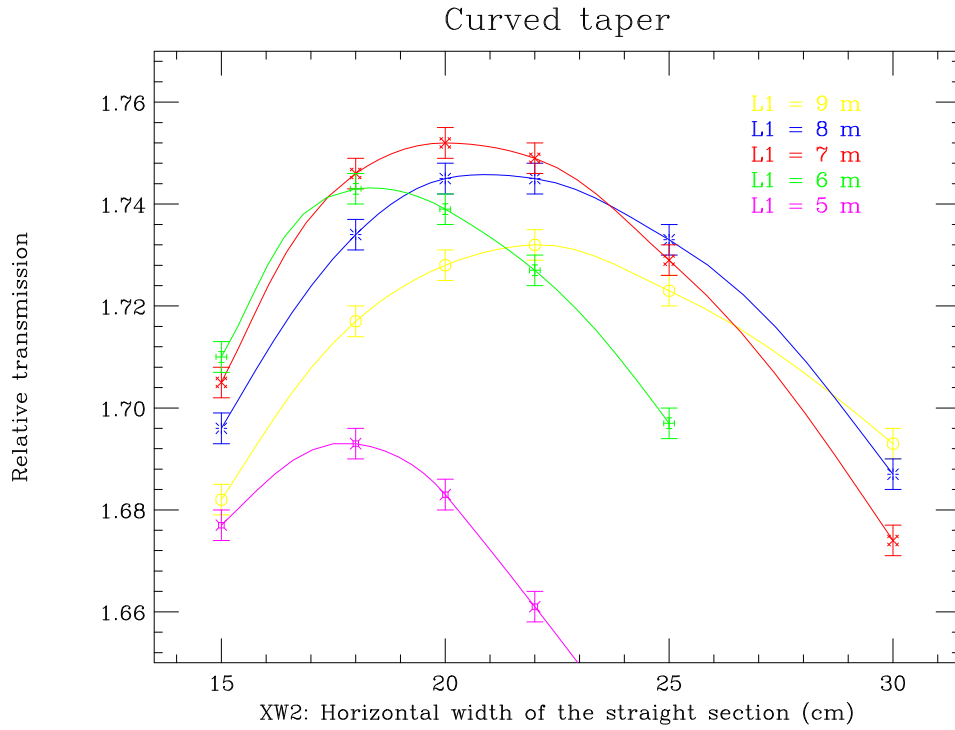


Fig. 10. Relative transmission vs horizontal width of the straight section for geometries with curved taper.

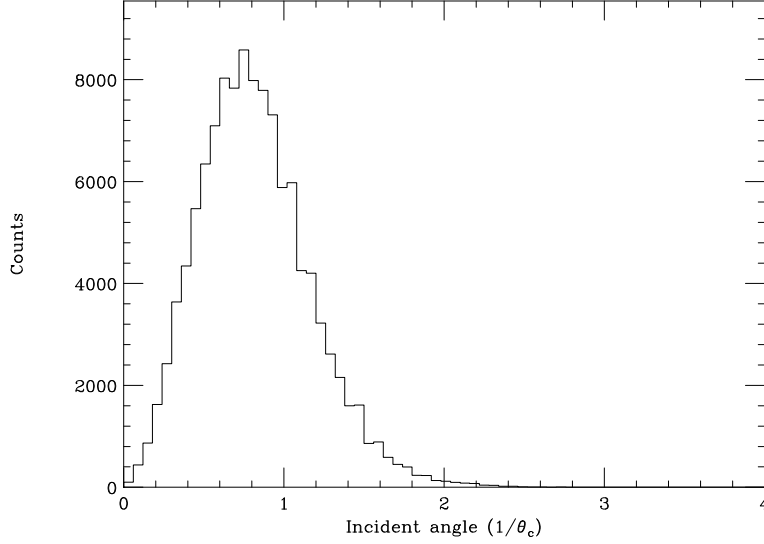


Fig. 11. Distribution of the incident angle of the neutrons on the side wall of the diverging horn. (For this plot, a geometry with $L1 = 8$ m and $XW2 = 20$ cm with straight taper was used as an example.)

of the neutrons right after the diverging horn, which are shown in Fig. 12. We further confirmed the validity of these choices by varying the values of these two m 's and seeing negligible increase in the output neutron flux when the values of the m 's were increased and seeing a significant reduction in the output neutron flux when the values of the m 's were decreased. For the converging horn, based on the discussion given in Section 2.1, it is important to use the largest possible value of m . Therefore, we decided to use $m3_{TB} = 3.5$, $m3_{LR} = 3.5$. It was confirmed by actual Monte Carlo calculations that lowering these m 's significantly decreases the output neutron flux. Reducing the m for the side walls of the diverging horn and the straight section from $m1_{LR} = 3.5$ and $m2_{LR} = 2.0$ to $m1_{LR} = 2.0$ and $m2_{LR} = 1.5$ reduced the guide price by $\sim 150,000$ USD or more, which is a substantial cost saving.

Figure 9 shows that geometries with straight taper favor a large $L1$, with $L1 = 8$ m and $L1 = 9$ m being the optimum. On the other hand, Figure 10 shows that geometries with curved taper favor a shorter $L1$, with $L1 = 7$ m giving the maximum relative transmission (with $XW2 = 20$ cm).

To see the effect of curved taper, let us compare Fig. 12 and Fig. 13. These Figures contain the horizontal and vertical angular distributions of neutrons exiting the diverging horn for a guide geometry with curved taper (Fig. 12) and straight taper (Fig. 13). Geometries with $L1 = 7$ m and $XW2 = 20$ cm are used here as examples. Although for the horizontal angular distribution the curved taper does not make a big difference because of the rather narrow initial distribution, it makes an obvious difference for the vertical distribution. Both of the two effects that were discussed in Section 2.2 can be seen, i.e., a smaller loss in the diverging horn, and a more favorable angular distribution

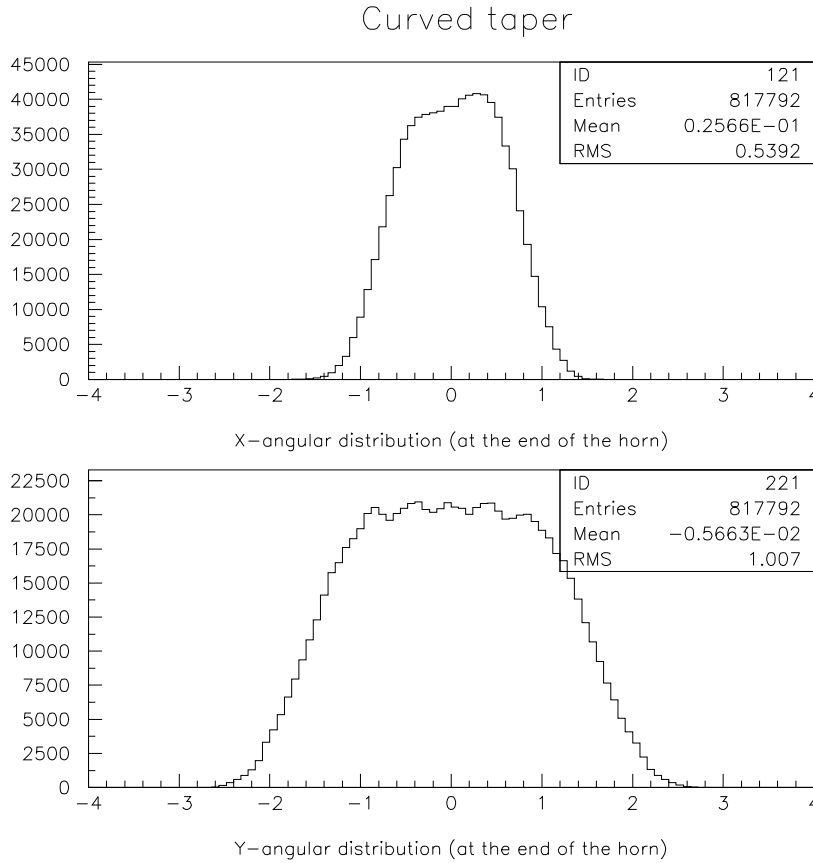


Fig. 12. Horizontal (top) and vertical (bottom) position distributions of the neutrons in the ballistic guide right after the diverging horn with curved taper. The angles are in the unit of θ_c . (For this plot, a geometry with $L1 = 7$ m, $XW2 = 20$ cm, $m1_{TB} = 3.5$, $m1_{LR} = 2.0$ was used as an example.)

after the diverging horn. The transmission through the diverging horn is 82% for curved taper, compared to 77% for the straight taper and the difference in the vertical angular distribution is obvious.

Coming back to Figs. 9 and 10, from these figures we observe the following three points:

- By using a ballistic guide we obtain a substantial gain in neutron flux ($\sim 55\%$ for straight taper and $\sim 75\%$ for curved taper as compared to the straight guide).
- Ballistic guides with curved taper give higher a output neutron flux than ballistic guides with straight taper.
- The optimum horizontal width for the straight section is around 20 cm (slightly narrower than expected based on a naive argument given in Section 2.1).

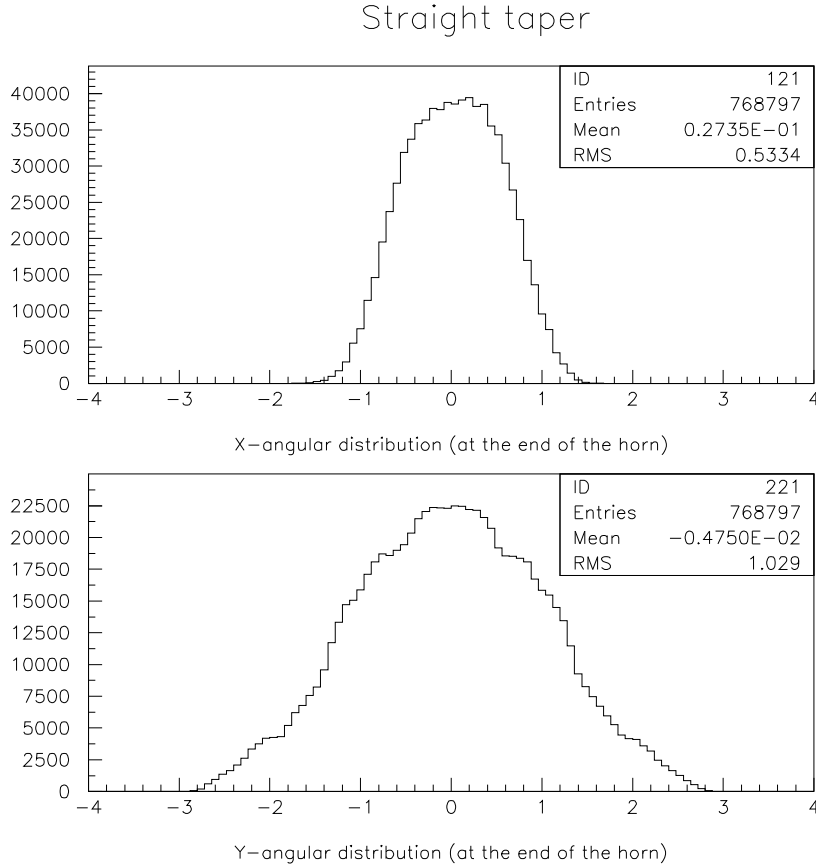


Fig. 13. Horizontal (top) and vertical (bottom) angular distributions of the neutrons in the ballistic guide right after the diverging horn straight taper. The angles are in units of θ_c . (For this plot, a geometry with $L1 = 7$ m, $XW2 = 20$ cm, $m1_{TB} = 3.5$, $m1_{LR} = 2.0$ was used as an example.)

In Table 4, the fraction of neutrons lost in various places in the ballistic guide are listed for the optimum geometry with curved taper and for the optimum geometry with straight taper. As expected, the use of the curved taper reduces the loss in the diverging and converging horns.

3.5 Full optimization

In order to verify the results of the physics motivated optimization, we proceeded to do a full-scale optimization of the ballistic guide geometry, fitting for as many degrees of freedom as possible. Two goals of this optimization were a) to investigate the effect of the shape of the diverging and converging horns, and b) to verify that the two horns should indeed be symmetric.

Table 4

Fractions of neutrons lost in various places in the ballistic guide for the optimum geometry with curved taper and for the optimum geometry with straight taper

Description	Curved taper	Straight taper
Lost in the diverging horn (left or right walls)	0.005	0.006
Lost in the diverging horn (top or bottom walls)	0.177	0.243
Lost in the straight section (left or right walls)	0.008	0.007
Lost in the straight section (top or bottom walls)	0.052	0.049
Lost in the converging horn (left or right walls)	0.008	0.008
Lost in the converging horn (top or bottom walls)	0.053	0.066
Survived	0.697	0.622

To investigate the shape of the horn, a cubic term was added to Eq. 2:

$$\hat{x} = \hat{z} [1 + a(1 - \hat{z}) (1 + b(1 - \hat{z}))], \quad (3)$$

in normalized coordinates $0 < \hat{x} < 1$ and $0 < \hat{z} < 1$, where $x = X_1 + |X_2 - X_1| \hat{x}$ and $z = L_1 + |L_2 - L_1| \hat{z}$. The coordinates (X_1, L_1) are at the entrance/exit of the horn, while (X_2, L_2) connect to the straight section. The cubic term with coefficient b was added in such a way that it reduces to Eq. 2 in the limit $b = 0$, to a straight line in the limit $a = 0$, and has the same slope $m = 1 - a$ at the end of the horn ($z = L_2$). By imposing the constraint of no inflection points over the length of the horn, the cubic term is limited to the range $-\frac{1}{2} < b < 1$. This extra term allows one to match up the slope of the horn with the straight section ($a = 1$) while simultaneously adjusting the slope at $z = 0$ within the range $\frac{3}{2} < d\hat{x}/d\hat{z} < 3$.

Noting the large difference between a_H and a_V in Table 3, a second parameter $c = L_V/L_H - 1$ was added, relaxing the curved horn to have different lengths in the horizontal and vertical sides. The purpose of this additional parameter was to ensure that the shape of the horn in the vertical direction was not constrained by its horizontal length. Separate parameters a_H , a_V , b_H , b_V , and c were optimized for both the diverging and converging horns.

The multiparameter optimization was done using a custom computer code MI-NOISE based on the conjugate gradient technique (Ref.[7], sec. 10.6). The line minimization algorithm was modified to handle uncertainty in the minimization function (the transmission) due to statistical errors associated with the Monte Carlo technique. Instead of bracketing and searching for the minimum by golden means, the transmission is sampled at n points along the line, and

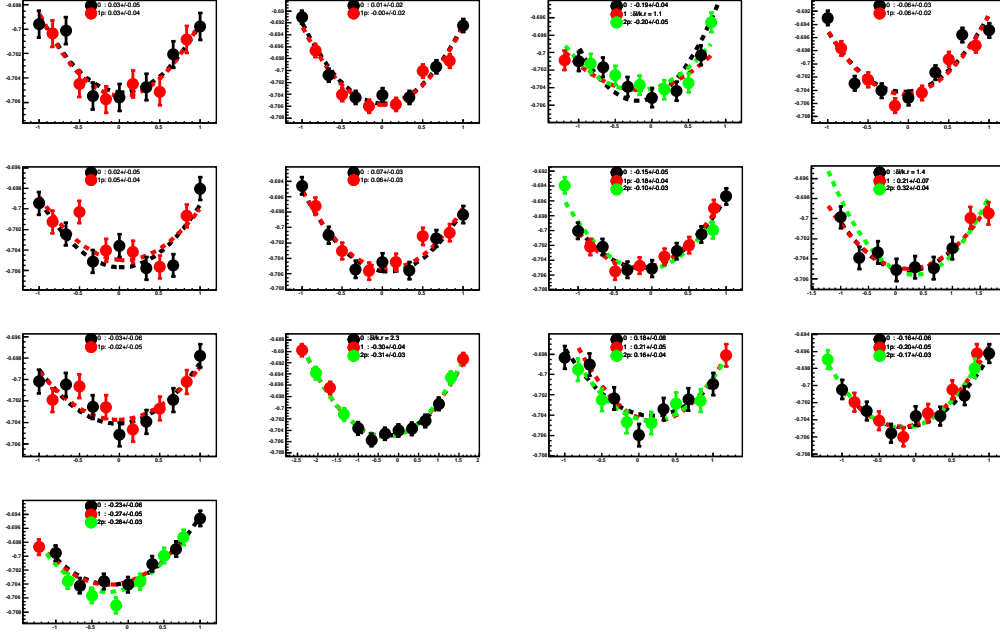


Fig. 14. Graphical output of a multiparameter optimization of MINOSE.

fit for the parabolic minimum. The algorithm also has the capability to: a) narrow the range if χ^2 of the fit is too large; b) zoom out if uncertainty in the minimum is too large or the parabola has the wrong curvature; c) recenter the range on the minimum, adding extra points to fill in the gaps; and d) increase the density of points for the final fit after finding the range. Because of the cost of each Monte Carlo simulation, care was taken to reuse old points and only do new simulations where necessary. In order to perform the 400 – 1500 Monte Carlo simulations necessary for a full parameter optimization, the NEUTRACK 8.9 based ballistic guide simulation described in section 3.3 was executed from an MPI [8] wrapper, and run in parallel on a 40 CPU farm. In this manner, simulations of 200000 events could be run in less than 5 s each. The graphical output of a minimization of 13 parameters is shown in Fig. 14. Different colors represent different range-finding iterations.

Three optimizations were carried out, listed in Table 5. The first optimization was done to find the optimal height of the guide, $YW2 = 37.6$ cm. This is very close to the limit of 30 cm, and the transmission changed very little to due this constraint. The second optimization verified the values of L and a determined in the physics-motivated section, and showed that the guide should be reasonably symmetric along its length. The third fit, a full-parameter optimization, improved very little over the previously obtained transmission. This supports the above arguments that the guide performance is insensitive to the details of its curvature, and shows that the guide is well-optimized for the angular distribution of neutrons at the source. In fact, very little transmission was gained by increasing the m -value of the supermirrors in the diverging horn.

Table 5

Multiparameter optimizations of transmission: line 1) fit of optimal guide height, 2) verification of conventional parameters, 3) fit for extra curvature parameters.

	diverging horn						straight		converging horn					TXMIT	
	<i>L1</i>	<i>a_H</i>	<i>a_V</i>	<i>b_H</i>	<i>b_V</i>	<i>c</i>	<i>XW</i>	<i>YW</i>	<i>L3</i>	<i>a_H</i>	<i>a_V</i>	<i>b_H</i>	<i>b_V</i>	<i>c</i>	
1)	8.8	.22	1.14	—	—	—	.218	.376	9.3	.58	1.25	—	—	—	74.4
2)	7.2	.29	1.16	—	—	—	.202	—	7.4	.61	1.10	—	—	—	70.2
3)	8.4	.20	1.16	-.15	.53	-.056	.206	—	8.2	.57	1.12	.49	.17	-.038	70.5

4 Summary

The design for the ballistic guide for the FNPB 8.9 Å neutron line was optimized using Monte Carlo simulation. A simulation program written using NEUTRACK 8.9, a neutron ray tracing package specially developed for this purpose. It was shown that it is possible to increase the output neutron flux (and fluence) by more than 70% (as compared to that obtained by the straight guide) by using a ballistic guide with curved taper. With a properly designed ballistic guide, a neutron fluence of 1.65×10^9 n/s/Å is expected, which should be compared to 0.94×10^9 n/s/Å, a fluence expected for the straight guide.

5 Acknowledgments

We thank P. Huffman for valuable suggestions. This work was supported in part by US Department of Energy Division of Nuclear Physics through grant number DE-FG02-03ER41258.

References

- [1] F. Mezei, J. Neutron Res. **6**, 3 (1997).
- [2] The Spallation Neutron Source, <http://www.sns.gov/>.
- [3] Fundamental Neutron Physics Beamline, <http://www.phy.ornl.gov/nuclear/neutrons/>.
- [4] P. R. Huffman, *et al.*, J. Res. Natl. Inst. Stand. Technol. **110**, 161 (2005); P. R. Huffman, *et al.*, *Beamline Performance Simulations for the Fundamental Neutron Physics Beamline*, 2005 (unpublished).
- [5] McSTAS – A neutron ray-trace simulation package, <http://neutron.risoe.dk/>.

- [6] P. R. Huffman (private communication).
- [7] W. H. Press, *et al.*, *Numerical Recipes in C*, Cambridge University Press, (1988).
- [8] MPI – Message Passing Interface, <http://www.mcs.anl.gov/mpi/mpich>.